# Origin of the Phase Transition in Lithiated Molybdenum Disulfide
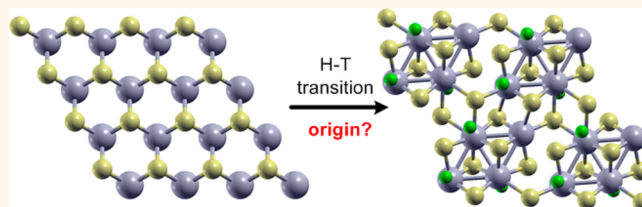
Yingchun Cheng,[†,§] Anmin Nie,[‡,§] Qingyun Zhang,[†] Li-Yong Gan,[†] Reza Shahbazian-Yassar,[*,‡] and Udo Schwingenschlögl[*,†]

[†]Department of Materials Science and Engineering, King Abdullah University of Science & Technology, Thuwal, 23955-6900, Kingdom of Saudi Arabia and [‡]Department of Mechanical Engineering-Engineering Mechanics, Michigan Technological University, 1400 Townsend Dive, Houghton, Michigan 49931, United States. [§]Y.C. and A.N. contributed equally to this work.

**ABSTRACT** Phase transitions and phase engineering in two-dimensional $MoS_2$ are important for applications in electronics and energy storage. By *in situ* transmission electron microscopy, we find that $H\text{-}MoS_2$ transforms to $T\text{-}LiMoS_2$ at the early stages of lithiation followed by the formation of Mo and $Li_2S$ phases. The transition from $H\text{-}MoS_2$ to $T\text{-}LiMoS_2$ is explained in terms of electron doping and electron−phonon coupling at the conduction band minima. Both



are essential for the development of two-dimensional semiconductor-metal contacts based on $MoS_2$ and the usage of $MoS_2$ as anode material in Li ion batteries.

**KEYWORDS:** phase transition · dichalcogenide · electron−phonon coupling · battery

Molybdenum disulfide ($MoS_2$), which is composed of atomic slabs bound by van der Waals forces, has been used as solid lubricant for decades,[1,2] for example, in the windshield wiper blades of vehicles. It also has potential applications related to the hydrogen evolution reaction,[3,4] Li ion batteries,[5−7] and supercapacitors.[8−10] Owing to its layered structure, $MoS_2$ can be mechanically exfoliated into single layers, showing an indirect-to-direct band gap transition in this limit.[11,12] Moreover, because of the strong spin orbit coupling and inversion symmetry breaking, a huge spin splitting appears at the K valleys in single layer $MoS_2$,[13] which is promising in spintronics, valleytronics, and optoelectronics.[14−19] Nevertheless, probably the most important application of $MoS_2$ is found in Li ion batteries, for which structural aspects and possible phase transitions are key issues. A detailed review on the state-of-the-art in this field recently has been presented by Stephenson and co-workers.[20]

The most common phase of $MoS_2$ has a trigonal structure (ABAB stacking, 2H phase), where the S atoms form hexagonal close-packed layers and the Mo atoms are located between S layers. Because of the weak interlayer interaction, also a 3R phase with ABCABC stacking can be fabricated by chemical vapor deposition.[20] Single layer $H\text{-}MoS_2$ has been achieved by exfoliation[21] and chemical vapor deposition.[22] Recently, another polytype, the T phase, has been observed in Li ion intercalated $MoS_2$,[23,24] being metallic, as demonstrated by photoluminisence experiments.[25] However, there remain debates, particularly, concerning the claim that $MoS_2$ realizes the T phase after Li intercalation,[23,24] which contradicts first-principles findings that this phase is unstable,[26] Therefore, it is important to obtain insight into the origin of the H−T phase transition in lithiated $MoS_2$. Deep lithiation leads to Mo cluster formation,[27] for which the mechanism and effects on the cyclability of Li ion batteries are not clear so far.[28]

In this work, we demonstrate an H−T phase transition in the early lithiation process of $MoS_2$. First-principles calculations show that the T phase refers to $LiMoS_2$ rather than $MoS_2$ and that the transition can be attributed to an unusual interplay of intrinsic doping and electron−phonon coupling. Under deep lithiation, $T\text{-}LiMoS_2$ transforms into $Li_2S$ and Mo clusters, where the latter enhance the $Li_2S\text{−}S$ cyclability in Li ion batteries.
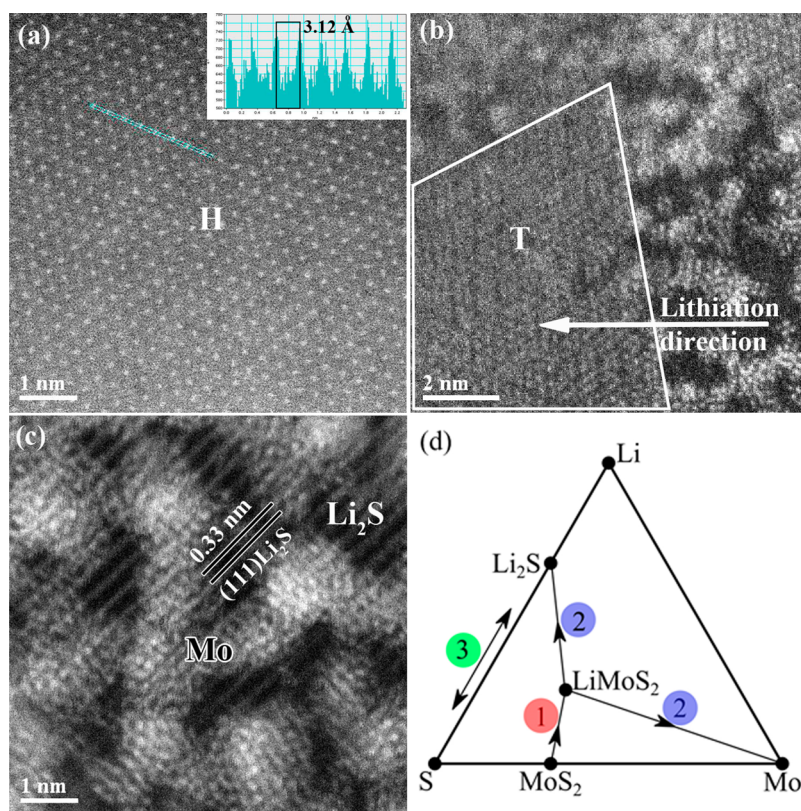
Figure 1. (a) Scanning TEM high-angle annular dark-field image of 2H-MoS$_2$ in the pristine state (without Li). Inset is the intensity profile along the marked line. (b) T phase after slight lithiation (bottom left area) with some Mo clusters and Li$_2$S. (c) Under deep lithiation the T phase disappears and only Mo clusters and Li$_2$S are left. (d) Species phase diagram, where ① indicates the formation of LiMoS$_2$ in the early lithiation process, ② is the formation of Mo and Li$_2$S under deep lithiation, and ③ is further de(lithiation) related to Li$_2$S.

## RESULTS AND DISCUSSION

Figure 1a shows the H phase of MoS$_2$ without Li intercalation. Fast Fourier transformation of the square area shows a 6-fold symmetry ($a^* = b^*$) (see Supporting Information, Figure S1a). The Mo—Mo distance is measured to be 3.12 Å (see the intensity profile in the image), which is consistent with the inorganic crystal structure database (ICSD) value of 3.16 Å as well as with our calculated value of 3.17 Å. After Li intercalation, Mo slightly dimerizes in the ab-plane (Figure 1b and the T phase in Figure 2b. Fast Fourier transformation of the square area shows, for a partially lithiated MoS$_2$ super-structure, reflections at $0.5a^*$ (Figure S1b), which point to a $2a \times 2a$ superstructure. The arrangement of the Mo atoms (T phase) in the box area in Figure 1b is in good agreement with the 1T' phase of MoS$_2$ as reported by the previous experiments.[24] Further lithiation leads to Mo clusters and crystalline Li$_2$S (Figure 1c). The measured lattice spacing of 3.30 Å agrees well with the (111) planes of Li$_2$S in the ICSD (No. 060432). An investigation of MoS$_2$ nanosheets after lithiation by transmission electron microscopy (TEM) has revealed an H—T phase transition with Li occupying the inter-layer S—S tetrahedral site, the so-called 1T-LiMoS$_2$ phase,[27] without addressing details of the transition. Therefore, the question arises whether the T phase
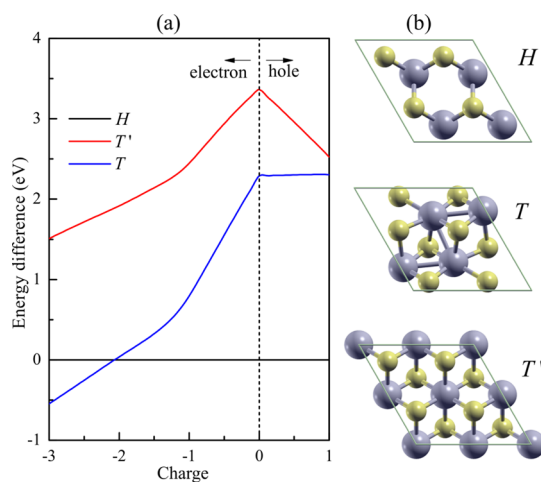


Figure 2. (a) Energy differences between the H phase and the T and T' phases of MoS$_2$ as a function of the charge (number of added/removed electrons). The three structures are shown in panel b. The yellow and blue balls represent the S and Mo atoms, respectively.

refers to MoS$_2$ or rather to LiMoS$_2$. Total energy and phonon dispersion calculations[26] indicate that T-MoS$_2$ is not stable, thus pointing to LiMoS$_2$. Figure 1d gives the species phase diagram of Li, Mo, and S based on the ICSD,[29] showing that LiMoS$_2$ can be formed only in the early lithiation process.
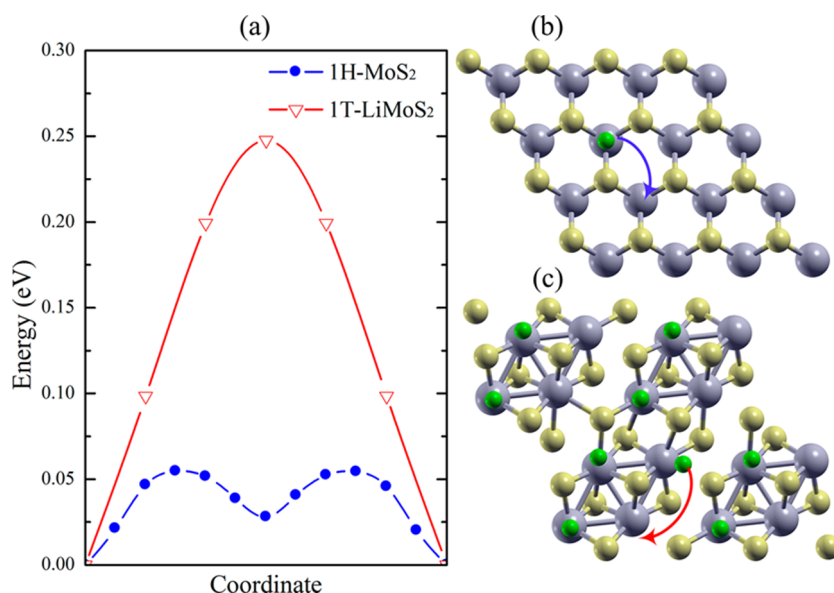
**Figure 3.** (a) Transition barriers for a Li atom in H-MoS$_2$ and T-LiMoS$_2$. (b,c) Migration paths. The yellow, blue, and green balls represent the S, Mo, and Li atoms, respectively.

For a single Li atom located on top of Mo in H-MoS$_2$ some charge is transferred to MoS$_2$ according to a Lowdin charge analysis. The T phase is also achieved by the substitutional doping of Re, Tc, and Mn atoms.[30] An H−T phase transition has been observed by scanning TEM for Re-doped MoS$_2$ (doping concentration < 1%) under high temperature (400−700 °C) in ref 31, but its origin and nature have not been addressed. Because Re has one more valence electron than Mo, one may assume that the H−T phase transition is due to the electron doping.

The stability of 2H- and 1T-LiMoS$_2$ has been investigated as a function of the Li content and intercalation sites.[32] Octahedral coordination in the van der Waals gap is found to be favorable for both allotropes. For simplicity, in the calculations we add/remove electrons to/from the pristine system to simulate doping. Figure 2a shows the obtained energy differences between the H phase and the T (distorted) and T′ (ordered) phases. We find that the T phase is favorable over the T′ phase in a large range of electron doping. For a doping of more than two electrons per 2 × 2 cell (5.76 × 10$^{14}$ cm$^{-2}$) the T phase is favorable over the H phase, which is consistent with our assumption above.

To determine the stable Li adsorption sites in H-MoS$_2$ and T-LiMoS$_2$, we address the binding energy ($E_b$). For adsorption on H-MoS$_2$ we have $E_b = E_{Li} + E_{MoS2} − E_{Li@MoS2}$, for which $E_{Li@MoS2}$, $E_{Li}$, and $E_{MoS2}$ are the energies of MoS$_2$ with adsorbed Li atom, a free Li atom, and single layer MoS$_2$, respectively. Considering the different absorption sites for MoS$_2$, $T_{Mo}$ (top of Mo), H (hollow), and $T_S$ (top of S), we find that $E_b$ for absorption at the $T_{Mo}$ site (0.90 eV) is 0.41 eV higher than for the H site and 0.21 eV higher than for the $T_S$ site. For LiMoS$_2$ the favorable absorption site is also $T_{Mo}$

($E_b$ = 0.92 eV). In general, the low value of $E_b$ reflects weak interaction between the Li atoms and H-MoS$_2$/T-LiMoS$_2$.

To evaluate the mobility of Li, we calculated the transition barriers between neighboring $T_{Mo}$ sites by nudged elastic band calculations,[33−35] obtaining 0.05 and 0.24 eV for H-MoS$_2$ and T-LiMoS$_2$, respectively. The transition coordinates are shown in Figure 3b,c. The transition barrier is much smaller for H-MoS$_2$ than for T-LiMoS$_2$, which indicates that the mobility of the Li atoms is higher on the H-MoS$_2$ surface than on the T-LiMoS$_2$ surface. After transformation of H-MoS$_2$ to T-LiMoS$_2$, therefore, extra Li atoms tend to accumulate in the dimerization gaps of T-LiMoS$_2$, see Figure 3c.

Some layered transition metal dichalcogenides, such as 1T-TiS$_2$ and 2H-TaSe$_2$, are metallic at room temperature but below a certain temperature develop a semiconducting charge density wave (CDW) phase due to Peierls distortions.[36] It has been claimed that the origin of the transition from H-MoS$_2$ to T-LiMoS$_2$ is also a CDW.[37] However, there are three aspects that contradict this picture. First, the transition is from semiconducting to metallic. Second, there is no CDW phase in H-MoS$_2$ without charge doping. Third, the structure not only undergoes a dimerization of the Mo atoms but also a sliding of the S planes. The atomic distortions are larger than found in the CDW phases of other transition metal dichalcogenides. Thus, it is necessary to further investigate the origin of the phase transition from H-MoS$_2$ to T-LiMoS$_2$.

Figure 4a,b show the band structure and density of states of single layer H-MoS$_2$ without considering the spin orbit coupling. The direct band gap of 1.7 eV is consistent with previous reports.[11−13] The energy map
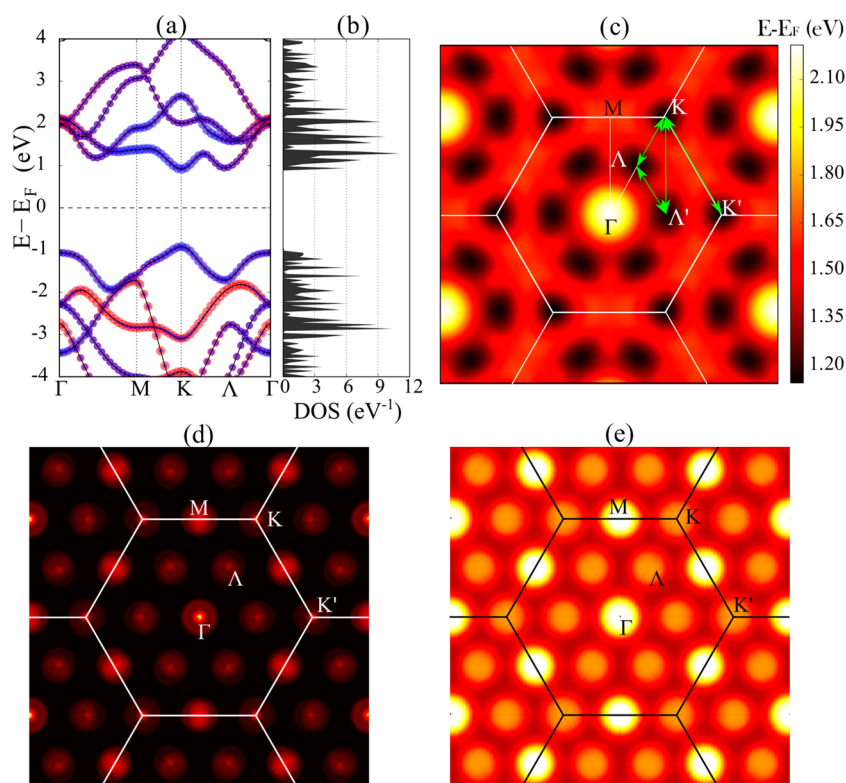
**Figure 4.** (a) Orbital projected band structure and (b) density of states of single layer H-MoS$_2$. Blue and red dots in panel a represent the Mo and S orbitals, respectively. (c) Energy map of the lowest conduction band. (d) Imaginary and (e) real part of the electronic susceptibility for electron doped ($1.15 \times 10^{14}$ cm$^{-2}$) single layer H-MoS$_2$.

of the lowest conduction band in Figure 4c shows two kinds of valleys (K valley and $\Lambda$ valley). The valence bands also give rise to two kinds of valleys (K valley and $\Gamma$ valley). Because H-MoS$_2$ is electron doped in our current study, we only consider the conduction band edge, for which the $\Lambda$ valley is 0.026 eV higher than the K valley. Using the density of states in Figure 4b, we estimate that the $\Lambda$ valley will be occupied with an electron concentration of more than $2.19 \times 10^{14}$ cm$^{-2}$ at zero temperature. If the electrons only occupy the K valley, see Figure 4c, the intervalley interaction would couple with phonons of wave vector K. If they also occupy the $\Lambda$ valley, the K and $\Lambda$ valleys and $\Lambda'$ and $\Lambda$ valleys would be coupled by phonons of wave vector $\Lambda$ and the K and $\Lambda'$ valleys by phonons of vector M. To obtain further insights, we study the real and imaginary parts of the electronic susceptibility for electron doped ($1.15 \times 10^{14}$ cm$^{-2}$) single layer H-MoS$_2$ using the constant matrix element approximation,[38] see Figure 4d,e. The imaginary part (nesting function) is very small, since the Fermi level is located near the conduction band minimum. Only weak peaks are found at the $\Gamma$, M, $\Lambda$, and K points. For the real part strong peaks show up near these points, caused by the modified Fermi level due to electron doping. The real part of the electronic susceptibility determines the stability of the electronic system, which couples to the lattice through electron–phonon interaction.

Figure 5a displays the phonon dispersion of uncharged single layer H-MoS$_2$. According to Figure 5b, an electron concentration of $1.15 \times 10^{14}$ cm$^{-2}$ results in phonon softening around the M, K, and $\Lambda$ points. For the M point one phonon branch even shows negative frequencies, pointing to instability against superconductivity. As this anomaly matches the pronounced peak of the real part of the electronic susceptibility, see Figure 4e, we can conclude that the electronic instability combined with strong electron–phonon interaction induces the phonon softening and thus the H–T phase transition. Since the M point is located at the Brillouin zone boundary ([0.5, 0, 0]) the distorted structure will have a larger 2 × 2 cell. The atomic displacements related to the soft phonon at the M point are shown in Figure 5c, where those for Mo are larger than those for S. According to the atomic displacements we build a distorted 2 × 2 supercell, in which neighboring unit cells have opposite displacements (see the dimerization of the Mo atoms in Figure 5d). Under relaxation this structure turns into the T phase structure with a significant reduction of the total energy.

As shown before, the critical Li concentration for the phase transition is $5.76 \times 10^{14}$ cm$^{-2}$. Energy difference calculations point to a phase transition at a concentration of 40%,[30,32] suggesting that H-MoS$_2$ transforms into T-LiMoS$_2$ suddenly at this value, whereas it is difficult to determine the critical concentration
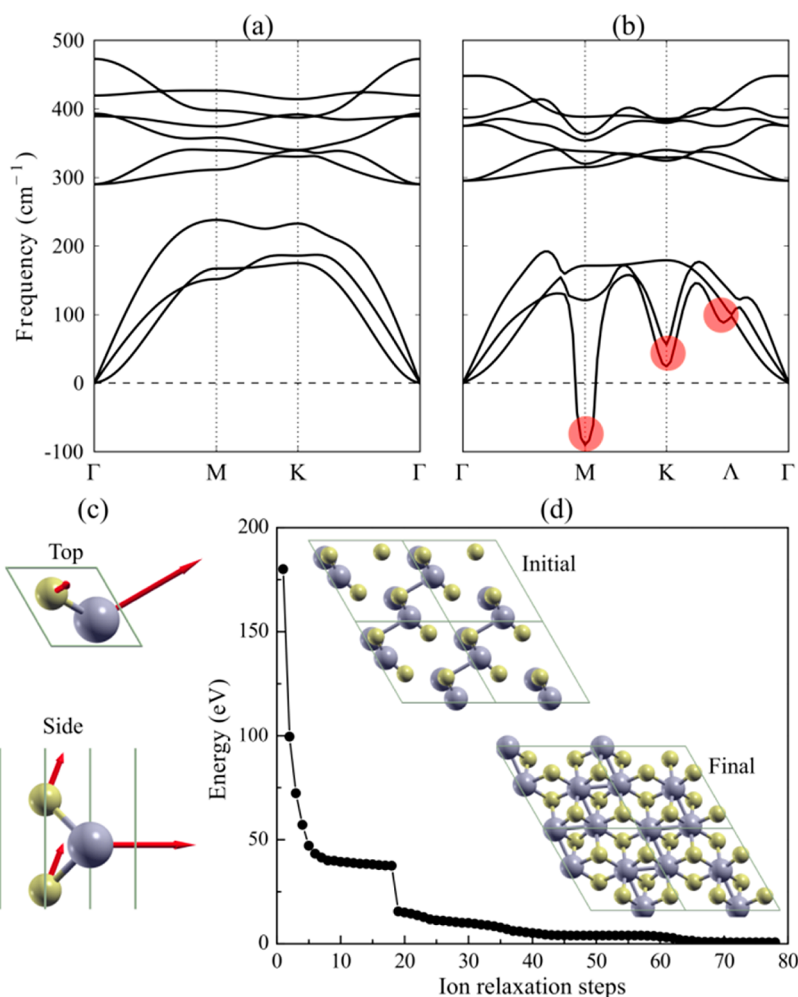
**Figure 5.** Phonon dispersions of (a) uncharged and (b) electron doped ($1.15 \times 10^{14}$ cm$^{-2}$) single layer H-MoS$_2$. (c) Top and side views of the atomic displacements of the soft mode at the M point in panel b. (d) Energy as a function of the ion relaxation steps for a $2 \times 2$ supercell. The initial structure is based on the atomic displacements shown in panel c. After full relaxation, the T phase of MoS$_2$ is established. The yellow and blue balls represent the S and Mo atoms, respectively.

experimentally by TEM. For the phase transition in Re-doped MoS$_2$ it is about 30%−40% according to energy difference calculations,[30] which is much higher than the experimental result (<1%).[31] Apparently, the critical concentration for the H−T phase transition is dramatically overestimated by energy difference calculations. Considering the electron−phonon interaction, we demonstrate (Figures 4 and 5) that a Li concentration of $1.15 \times 10^{14}$ cm$^{-2}$ is sufficient for the phase transition, which thus is rather continuous, consistent with previous reports.[39,40]

We characterize the clusters shown in Figure 1c by electron energy loss spectroscopy and find that the bright clusters in scanning TEM high-angle annular dark-field images (Supporting Information, Figure S2a) are due to Mo and the dark matrix is due to Li$_2$S. According to the species phase diagram shown in Figure 1d, we can expect formation of Mo and Li$_2$S for deep lithiation. A recent TEM study of postcycled MoS$_2$ electrodes has detected metallic Mo in the delithiated state.[41] The main limiting factor for applications of MoS$_2$

is the poor cyclability,[42,43] which results from the fact that it is difficult to form LiMo alloy. On the other hand, further de(lithiation) is related to Li$_2$S and S, see the reaction ③ in Figure 1d. This suggests the possibility of using MoS$_2$ in Li ion batteries. In the context of the low electroconductivity of S,[44] the formation of Mo clusters has the merit of providing a substantial enhancement.

## CONCLUSION

By *in situ* TEM, we find a phase transition from H-MoS$_2$ to T-LiMoS$_2$ in the early lithiation process of MoS$_2$ and later the formation of Mo and Li$_2$S clusters. The poor cyclability of anodes based on MoS$_2$ is attributed to the difficulty to form MoS$_2$ from Mo and Li$_2$S in the delithiation process. However, Mo clusters can enhance the electroconductivity of S in the Li$_2$S−S cycle. Simulations based on density functional theory show that the phase transition from H-MoS$_2$ to T-Li-MoS$_2$ is due to electron doping, in which the electronic structure and phonon dispersion indicate that the electron−phonon coupling in the conduction band

valleys plays a key role. The provided insights into the phase transition in electron-doped $MoS_2$ are important for phase engineering in energy storage and electronic applications.

## EXPERIMENTAL AND CALCULATIONAL DETAILS

***In Situ* Experiments.** $MoS_2$ nanosheets grown by chemical vapor deposition (serving as working electrode) were scraped away from an Si substrate by a gold wire. Li metal (serving as the counter electrode and Li source) was scratched by another gold wire inside a glovebox filled with Ar. The two electrodes were mounted onto a Nanofactory Instruments TEM *in situ* sample holder, which was transferred with an airtight container and loaded into the TEM column. The naturally grown $Li_2O$ layer on the surface of the Li metal served as solid electrolyte for the Li transport. The $Li_2O/Li$ electrode side was moved forward to contact the edge of the $MoS_2$ nanosheet. Once a reliable electrical contact was built, a potential ranging from $-2$ to $-4$ V was applied to the $MoS_2$ nanosheet to initiate the lithiation, which was stopped at various intermediate stages by retracting the Li source and electrolyte, see Supporting Information, Figure S3. The experiments were carried out inside an aberration-corrected JEOL JEM-ARM200CF scanning TEM equipped with a 200 keV Schottky cold-field emission gun, high-angle annular dark-field detectors, and a postcolumn Gatan Enfina electron energy loss spectrometer. A 22-mrad-probe convergence angle was used for all the images and spectra. The high-angle annular dark-field images were acquired using a 90 mrad inner detector angle, and the electron energy loss spectra was acquired using a 45 mrad collection angle.

**Ab Initio Simulations.** All calculations were performed using the Quantum-ESPRESSO package[45] in the framework of density functional theory. Ultrasoft pseudopotentials[46] as well as the generalized gradient approximation in the Perdew−Burke−Ernzerhof parametrization[47] of the exchange correlation functional were employed. A self-consistency energy accuracy of $1.4 \times 10^{-9}$ eV, residual forces below $2.6 \times 10^{-3}$ eV/Å, and a total energy convergence of $1.4 \times 10^{-4}$ eV were achieved. A 15 Å thick vacuum layer was adopted to prevent self-interaction by the periodic boundary conditions and the lattice constant of $H$-$MoS_2$ was used also for T- and T′-$MoS_2$. The phonon dispersions were obtained from density functional perturbation theory.[48]

*Conflict of Interest:* The authors declare no competing financial interest.

*Supporting Information Available:* The structure evolution during the lithiation of $MoS_2$ is demonstrated in Figure S1 by means of Fast Fourier transformation. Figure S2 shows high-angle annular dark-field and electron energy loss spectroscopy maps. A schematic view of the contact of the $Li_2O/Li$ electrode with the $MoS_2$ nanosheets is given in Figure S3. This material is available free of charge *via* the Internet at http://pubs.acs.org.

## REFERENCES AND NOTES

1. Holinski, R.; Gansheim, J. A Study of Lubricating Mechanism of Molybdenum Disulfide. *Wear* **1972**, *19*, 329–342.
2. Winer, W. O. Molybdenum Disulfide as a Lubricant—A Review of Fundamental Knowledge. *Wear* **1967**, *10*, 422–452.
3. Kibsgaard, J.; Chen, Z. B.; Reinecke, B. N.; Jaramillo, T. F. Engineering the Surface Structure of $MoS_2$ to Preferentially Expose Active Edge Sites for Electrocatalysis. *Nat. Mater.* **2012**, *11*, 963–969.
4. Wang, H. T.; Lu, Z. Y.; Kong, D. S.; Sun, J.; Hymel, T. M.; Cui, Y. Electrochemical Tuning of $MoS_2$ Nanoparticles on Three-Dimensional Substrate for Efficient Hydrogen Evolution. *ACS Nano* **2014**, *8*, 4940–4947.
5. Das, S. K.; Mallavajula, R.; Jayaprakash, N.; Archer, L. A. Self-Assembled $MoS_2$-Carbon Nanostructures: Influence of Nanostructuring and Carbon on Lithium Battery Performance. *J. Mater. Chem.* **2012**, *22*, 12988–12992.
6. Hwang, H.; Kim, H.; Cho, J. $MoS_2$ Nanoplates Consisting of Disordered Graphene-like Layers for High Rate Lithium Battery Anode Materials. *Nano Lett.* **2011**, *11*, 4826–4830.
7. Wang, S. Q.; Li, G. H.; Du, G. D.; Li, L.; Jiang, X. Y.; Feng, C. Q.; Guo, Z. P.; Kim, S. Synthesis and Characterization of Cobalt-Doped $WS_2$ Nanorods for Lithium Battery Applications. *Nanoscale Res. Lett.* **2010**, *5*, 1301–1306.
8. Huang, K. J.; Wang, L.; Liu, Y. J.; Liu, Y. M.; Wang, H. B.; Gan, T.; Wang, L. L. Layered $MoS_2$-Graphene Composites for Supercapacitor Applications with Enhanced Capacitive Performance. *Int. J. Hydrogen Energy* **2013**, *38*, 14027–14034.
9. Huang, K. J.; Wang, L.; Liu, Y. J.; Wang, H. B.; Liu, Y. M.; Wang, L. L. Synthesis of Polyaniline/2-Dimensional Graphene Analog $MoS_2$ Composites for High-Performance Supercapacitor. *Electrochim. Acta* **2013**, *109*, 587–594.
10. Ma, G. F.; Peng, H.; Mu, J. J.; Huang, H. H.; Zhou, X. Z.; Lei, Z. Q. *In Situ* Intercalative Polymerization of Pyrrole in Graphene Analogue of $MoS_2$ as Advanced Electrode Material in Supercapacitor. *J. Power Sources* **2013**, *229*, 72–78.
11. Mak, K.; Lee, C.; Hone, J.; Shan, J.; Heinz, T. Atomically Thin $MoS_2$: A New Direct-Gap Semiconductor. *Phys. Rev. Lett.* **2010**, *105*, 136805.
12. Splendiani, A.; Sun, L.; Zhang, Y. B.; Li, T. S.; Kim, J.; Chim, C. Y.; Galli, G.; Wang, F. Emerging Photoluminescence in Monolayer $MoS_2$. *Nano Lett.* **2010**, *10*, 1271–1275.
13. Zhu, Z.; Cheng, Y.; Schwingenschlögl, U. Giant Spin-Orbit-Induced Spin Splitting in Two-Dimensional Transition-Metal Dichalcogenide Semiconductors. *Phys. Rev. B* **2011**, *84*, 153402.
14. Cao, T.; Wang, G.; Han, W. P.; Ye, H. Q.; Zhu, C. R.; Shi, J. R.; Niu, Q.; Tan, P. H.; Wang, E.; Liu, B. L.; *et al.* Valley-Selective Circular Dichroism of Monolayer Molybdenum Disulphide. *Nat. Commun.* **2012**, *3*, 887.
15. Feng, J.; Qian, X.; Huang, C.-W.; Li, J. Strain-Engineered Artificial Atom as a Broad-Spectrum Solar Energy Funnel. *Nat. Photonics* **2012**, *6*, 866–872.
16. Kim, S.; Konar, A.; Hwang, W. S.; Lee, J. H.; Lee, J.; Yang, J.; Jung, C.; Kim, H.; Yoo, J. B.; Choi, J. Y.; *et al.* High-Mobility and Low-Power Thin-Film Transistors Based on Multilayer $MoS_2$ Crystals. *Nat. Commun.* **2012**, *3*, 1011.
17. Wang, H.; Yu, L.; Lee, Y.-H.; Shi, Y.; Hsu, A.; Chin, M. L.; Li, L.-J.; Dubey, M.; Kong, J.; Palacios, T. Integrated Circuits Based on Bilayer $MoS_2$ Transistors. *Nano Lett.* **2012**, *12*, 4674–4680.
18. Wang, Q. H.; Kalantar-Zadeh, K.; Kis, A.; Coleman, J. N.; Strano, M. S. Electronics and Optoelectronics of Two-Dimensional Transition Metal Dichalcogenides. *Nat. Nanotechnol.* **2012**, *7*, 699–712.
19. Xiao, D.; Liu, G.-B.; Feng, W.; Xu, X.; Yao, W. Coupled Spin and Valley Physics in Monolayers of $MoS_2$ and Other Group-VI Dichalcogenides. *Phys. Rev. Lett.* **2012**, *108*, 196802.
20. Cheng, Y. C.; Yao, K. X.; Yang, Y.; Li, L.; Yao, Y. B.; Wang, Q. X.; Zhang, X. X.; Han, Y.; Schwingenschlogl, U. Van der Waals Epitaxial Growth of $MoS_2$ on $SiO_2/Si$ by Chemical Vapor Deposition. *RSC Adv.* **2013**, *3*, 17287–17293.
21. Lee, C.; Yan, H.; Brus, L. E.; Heinz, T. F.; Hone, J.; Ryu, S. Anomalous Lattice Vibrations of Single- and Few-Layer $MoS_2$. *ACS Nano* **2010**, *4*, 2695–2700.
22. Lee, Y. H.; Zhang, X. Q.; Zhang, W. J.; Chang, M. T.; Lin, C. T.; Chang, K. D.; Yu, Y. C.; Wang, J. T. W.; Chang, C. S.; Li, L. J.; *et al.* Synthesis of Large-Area $MoS_2$ Atomic Layers with Chemical Vapor Deposition. *Adv. Mater.* **2012**, *24*, 2320–2325.
23. Chhowalla, M.; Shin, H. S.; Eda, G.; Li, L. J.; Loh, K. P.; Zhang, H. The Chemistry of Two-Dimensional Layered Transition

Metal Dichalcogenide Nanosheets. *Nat. Chem.* **2013**, *5*, 263–275.

24. Eda, G.; Fujita, T.; Yamaguchi, H.; Voiry, D.; Chen, M. W.; Chhowalla, M. Coherent Atomic and Electronic Heterostructures of Single-Layer $MoS_2$. *ACS Nano* **2012**, *6*, 7311–7317.

25. Eda, G.; Yamaguchi, H.; Voiry, D.; Fujita, T.; Chen, M.; Chhowalla, M. Photoluminescence from Chemically Exfoliated $MoS_2$. *Nano Lett.* **2011**, *11*, 5111–5116.

26. Shirodkar, S. N.; Waghmare, U. V. Emergence of Ferroelectricity at a Metal-Semiconductor Transition in a 1T Monolayer of $MoS_2$. *Phys. Rev. Lett.* **2014**, *112*, 157601.

27. Wang, L.; Xu, Z.; Wang, W.; Bai, X. Atomic Mechanism of Dynamic Electrochemical Lithiation Processes of $MoS_2$ Nanosheets. *J. Am. Chem. Soc.* **2014**, *136*, 6693–6697.

28. Stephenson, T.; Li, Z.; Olsen, B.; Mitlin, D. Lithium Ion Battery Applications of Molybdenum Disulfide ($MoS_2$) Nanocomposites. *Energy Environ. Sci.* **2014**, *7*, 209–231.

29. Bergerhoff, G.; Hundt, R.; Sievers, R.; Brown, I. D. The Inorganic Crystal Structure Data Base. *J. Chem. Inf. Comp. Sci.* **1983**, *23*, 66–69.

30. Enyashin, A. N.; Yadgarov, L.; Houben, L.; Popov, I.; Weidenbach, M.; Tenne, R.; Bar-Sadan, M.; Seifert, G. New Route for Stabilization of 1T-$WS_2$ and $MoS_2$ Phases. *J. Phys. Chem. C* **2011**, *115*, 24586–24591.

31. Lin, Y.-C.; Dumcenco, D. O.; Huang, Y.-S.; Suenaga, K. Atomic Mechanism of the Semiconducting-to-Metallic Phase Transition in Single-Layered $MoS_2$. *Nat. Nanotechnol.* **2014**, *9*, 391–396.

32. Enyashin, A. N.; Seifert, G. Density-Functional Study of $Li_xMoS_2$ Intercalates ($0 \leq x \leq 1$). *Comput. Theor. Chem.* **2012**, *999*, 13–20.

33. Caspersen, K. J.; Carter, E. A. Finding Transition States for Crystalline Solid-Solid Phase Transformations. *Proc. Natl. Acad. Sci. U.S.A.* **2005**, *102*, 6738–6743.

34. Henkelman, G.; Jonsson, H. A Dimer Method for Finding Saddle Points on High Dimensional Potential Surfaces Using Only First Derivatives. *J. Chem. Phys.* **1999**, *111*, 7010–7022.

35. Weinan, E.; Ren, W. Q.; Vanden-Eijnden, E. String Method for the Study of Rare Events. *Phys. Rev. B* **2002**, *66*, 052301.

36. Zhu, Z. Y.; Cheng, Y. C.; Schwingenschlögl, U. Origin of the Charge Density Wave in 1T-$TiSe_2$. *Phys. Rev. B* **2012**, *85*, 245133.

37. Rocquefelte, X.; Boucher, F.; Gressier, P.; Ouvrard, G.; Blaha, P.; Schwarz, K. Mo Cluster Formation in the Intercalation Compound $LiMoS_2$. *Phys. Rev. B* **2000**, *62*, 2397–2400.

38. Johannes, M.; Mazin, I.; Howells, C. Fermi-Surface Nesting and the Origin of the Charge-Density Wave in $NbSe_2$. *Phys. Rev. B* **2006**, *73*, 205102.

39. Benavente, E.; Santa Ana, M. A.; Mendizabal, F.; Gonzalez, G. Intercalation Chemistry of Molybdenum Disulfide. *Coordin. Chem. Rev.* **2002**, *224*, 87–109.

40. Whittingham, M. S. Role of Ternary Phases in Cathode Reactions. *J. Electrochem. Soc.* **1976**, *123*, 315–320.

41. Zhou, X. S.; Wan, L. J.; Guo, Y. G. Facile Synthesis of $MoS_2$@CMK-3 Nanocomposite as an Improved Anode Material for Lithium-Ion Batteries. *Nanoscale* **2012**, *4*, 5868–5871.

42. Feng, C. Q.; Ma, J.; Li, H.; Zeng, R.; Guo, Z. P.; Liu, H. K. Synthesis of Molybdenum Disulfide ($MoS_2$) for Lithium Ion Battery Applications. *Mater. Res. Bull.* **2009**, *44*, 1811–1815.

43. Xiao, J.; Choi, D. W.; Cosimbescu, L.; Koech, P.; Liu, J.; Lemmon, J. P. Exfoliated $MoS_2$ Nanocomposite as an Anode Material for Lithium Ion Batteries. *Chem. Mater.* **2010**, *22*, 4522–4524.

44. Dean, J. A. *Lange's Handbook of Chemistry* 3rd ed.; McGraw-Hill Professional: New York, 1985.

45. Giannozzi, P.; Baroni, S.; Bonini, N.; Calandra, M.; Car, R.; Cavazzoni, C.; Ceresoli, D.; Chiarotti, G. L.; Cococcioni, M.; Dabo, I.; *et al.* QUANTUM ESPRESSO: A Modular and Open-Source Software Project for Quantum Simulations of Materials. *J. Phys.: Condens. Matter* **2009**, *21*, 395502.

46. Vanderbilt, D. Soft Self-Consistent Pseudopotentials in a Generalized Eigenvalue Formalism. *Phys. Rev. B* **1990**, *41*, 7892–7895.

47. Perdew, J. P.; Burke, K.; Ernzerhof, M. Generalized Gradient Approximation Made Simple. *Phys. Rev. Lett.* **1996**, *77*, 3865–3868.

48. Baroni, S.; de Gironcoli, S.; Dal Corso, A.; Giannozzi, P. Phonons and Related Crystal Properties from Density-Functional Perturbation Theory. *Rev. Mod. Phys.* **2001**, *73*, 515–562.